ISSN 1674-1056
http://cpb.iphy.ac.cn
http://iopscience.iop.org/cpb
中国物理 B
Chinese Physics
中国物理
Chinese Physics B

Noise temperature distribution of superconducting hot electron bolometer mixers

Kang-Min Zhou(周康敏), Wei Miao(缪巍), Yue Geng(耿悦), Yan Delorme, Wen Zhang(张文), Yuan Ren(任远), Kun Zhang(张坤), Sheng-Cai Shi(史生才)

Citation: Chin. Phys. B . 2020, 29(5): 058505 . **doi:** 10.1088/1674-1056/ab81f9
Journal homepage: http://cpb.iphy.ac.cn; http://iopscience.iop.org/cpb

What follows is a list of articles you may be interested in

Wavelength dependence of intrinsic detection efficiency of NbN superconducting nanowire single-photon detector

Yong Wang(王勇), Hao Li(李浩), Li-Xing You(尤立星), Chao-Lin Lv(吕超林), He-Qing Wang(王河清), Xing-Yu Zhang(张兴雨), Wei-Jun Zhang(张伟君), Hui Zhou(周慧), Lu Zhang(张露), Xiao-Yan Yang(杨晓燕), Zhen Wang(王镇)

Chin. Phys. B . 2019, 28(7): 078502 . **doi:** 10.1088/1674-1056/28/7/078502

Photon-counting chirped amplitude modulation lidar system using superconducting nanowire single-photon detector at 1550-nm wavelength

Hui Zhou(周慧), Yu-Hao He(何宇昊), Chao-Lin Lü(吕超林), Li-Xing You(尤立星), Zhao-Hui Li(李召辉), Guang Wu(吴光), Wei-Jun Zhang(张伟君), Lu Zhang(张露), Xiao-Yu Liu(刘晓宇), Xiao-Yan Yang(杨晓燕), Zhen Wang(王镇)

Chin. Phys. B . 2018, 27(1): 018501 . **doi:** 10.1088/1674-1056/27/1/018501

High efficiency, large-active-area superconducting nanowire single-photon detectors

Gu Min, Zhang La-Bao, Kang Lin, Zhao Qing-Yuan, Jia Tao, Wan Chao, Xu Rui-Ying, Yang Xiao-Zhong, Wu Pei-Heng, Zhang Yong, Xia Jin-Song

Chin. Phys. B . 2015, 24(6): 068501 . **doi:** 10.1088/1674-1056/24/6/068501

SPECIAL TOPIC — Terahertz physics

Noise temperature distribution of superconducting hot electron bolometer mixers*

Kang-Min Zhou(周康敏)[1,2], Wei Miao(缪巍)[1,2], Yue Geng(耿悦)[1,2,4], Yan Delorme[3], Wen Zhang(张文)[1,2], Yuan Ren(任远)[1,2], Kun Zhang(张坤)[1,2], and Sheng-Cai Shi(史生才)[1,2,†]

[1] *Purple Mountain Observatory, Chinese Academy of Sciences, Nanjing* 210023, *China*
[2] *Key Laboratory of Radio Astronomy, Chinese Academy of Sciences, Nanjing* 210023, *China*
[3] *Observatoire de Paris*, 75014 *Paris, France*
[4] *University of Science and Technology of China, Hefei* 230026, *China*

(Received 9 December 2019; revised manuscript received 17 January 2020; accepted manuscript online 23 March 2020)

We report on the investigation of optimal bias region of a wide-band superconducting hot electron bolometer (HEB) mixer in terms of noise temperature performance for multi-pixel heterodyne receiver application in the 5-meter Dome A Terahertz Explorer (DATE5) telescope. By evaluating the double sideband (DSB) receiver noise temperature ($T_{\rm rec}$) across a wide frequency range from 0.2 THz to 1.34 THz and with a large number of bias points, a broad optimal bias region has been observed, illustrating a good bias applicability for multipixel application since the performance of the HEB mixer is uniquely determined by each bias point. The noise temperature of the HEB mixer has been analyzed by calibrating the noise contribution of all RF components, whose transmissions have been measured by a time-domain spectroscopy. The corrected noise temperature distribution shows a frequency independence relation. The dependence of the optimal bias region on the bath temperature of the HEB mixer has also been investigated, the bath temperature has limited effect on the lowest receiver noise temperature until 7 K, however the optimal bias region deteriorates obviously with increasing bath temperature.

Keywords: superconducting hot electron bolometer (HEB) mixer, noise temperature distribution, bath temperature dependence, frequency dependence

PACS: 85.25.Pb, 85.25.Am **DOI:** 10.1088/1674-1056/ab81f9

1. Introduction

Superconducting hot electron bolometer (HEB) mixers[1] have been widely used in ground-based[2] and space-based observatories[3] due to the advantages of high sensitivity and low local oscillator (LO) power requirement comparing to other THz detectors.[4–6] The use of multipixel receivers can improve the mapping speed of the telescope significantly compared with that with single pixel beam receivers. Superconducting HEB mixer array has and will be used in several telescopes such as GLT,[7] upGREAT,[8] GUSTO,[9] and FIRSPEX.[10] Since Dome A holds the best terahertz window on the earth,[11] 5-meter Dome A Terahertz Explorer (DATE5) is proposed by Purple Mountain Observatory and a 1×4 superconducting HEB mixer array has been chosen as the mixer for the 200 μm wavelength band.

Due to the extreme environment at Dome A, the DATE5 telescope will be unmanned. For the 1×4 beams heterodyne receiver array, a DC bias reuse technology will also be applied to reduce the complexity of the bias system. What is more, it is difficult to get a uniformed LO power distribution for each pixel,[12,13] and the operation point of each superconducting HEB mixer is uniquely determined by the absorbed LO power, DC bias voltage, and bath temperature. Therefore, it becomes important to study the noise temperature distribution of superconducting HEB mixers for the multipixel application in DATE5 telescope.

Previous research[11] has proved that Dome A has good transmittance at frequency beyond 7 THz. Considering the possible application of HEB mixer in far-infrared frequency range, we investigated the frequency dependence of the optimal bias region of a wideband superconducting HEB mixer.

2. Experiment system

2.1. HEB mixer design

The 0.2–2 THz superconducting HEB device consists of a NbN micro-bridge and a planar spiral antenna. The NbN micro-bridge, located at the center of the planar spiral antenna, has a width of 2 μm and a length of 0.2 μm. The thickness of the NbN film is 5.5 nm and is connected to the spiral antenna by two Ti/Au pads. Both micro-bridge and spiral antenna are fabricated on the high-resistivity silicon substrate.

*Project supported by the Chinese Academy of Sciences (Grant Nos. GJJSTD20180003 and QYZDJ-SSW-SLH043), the National Key Basic Research and Development Program of China (Grant Nos. 2017YFA0304003 and 2018YFA0404701), the National Natural Science Foundation of China (Grant Nos. 11603081, 11673073, U1831202, and 11873099), and PICS projects between the CAS and the CNRS.

†Corresponding author. E-mail: scshi@pmo.ac.cn

© 2020 Chinese Physical Society and IOP Publishing Ltd

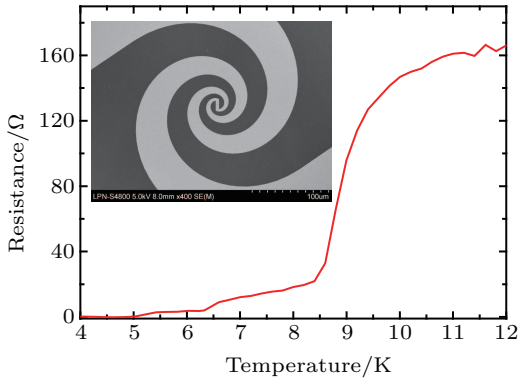


Fig. 1. Measured *R*–*T* curve of the superconducting HEB mixer. The inset presents the SEM picture of the log-spiral antenna coupled HEB device. The light gray area is the planar antenna, and the dark gray area is the Si substrate.

Figure 1 presents the SEM picture (inset image) of the superconducting HEB device. The spiral antenna arms are defined by $r_1 = ke^{a\varphi}$ and $r_2 = ke^{a(\varphi-\delta)}$, where $r_1 = 120$ μm is the outer radius, $r_2 = 3.6$ μm is the inner radius, $k = 4$ μm is the initial inner radius, $a = 0.35$ is the growth rate, and φ is the angular position. The simulated input resistance and reactance of the spiral antenna are shown in Fig. 2, the resistance is nearly constant (~ 80 Ω) in the whole operating frequency range.

The measured *R*–*T* and *I*–*V* curves of the HEB device are presented in Figs. 1 and 3, respectively. The critical temperature T_c is around 9 K, and the critical current I_c is around 100 μA at 4 K. The normal state resistance is about 160 Ω, as shown in Fig. 1.

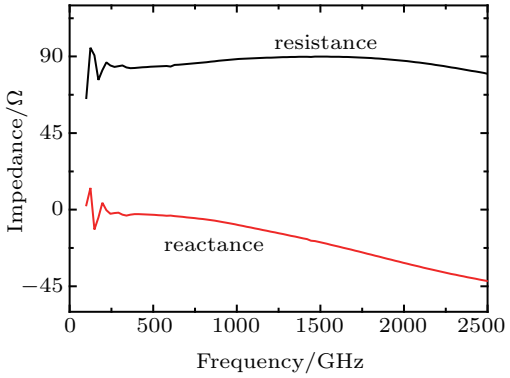


Fig. 2. Simulated input impedance of the log-spiral antenna.

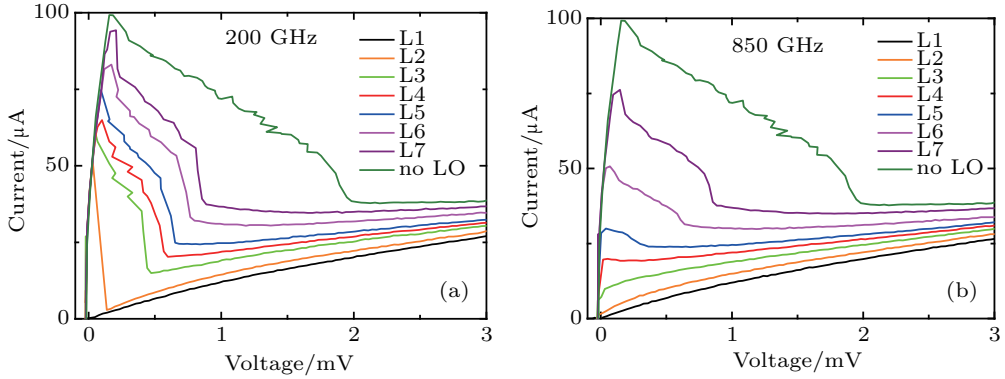


Fig. 3. The *I*–*V* curves at different pumping levels at (a) 0.2 THz and (b) 0.85 THz, negative resistance can still be found even at well-pumped *I*–*V* curves at 0.2 THz.

2.2. Measurement setup

The double sideband (DSB) receiver noise temperatures of the 0.2–2 THz HEB mixer are measured at 0.2 THz, 0.5 THz, 0.85 THz, and 1.34 THz by the *Y*-factor method. The measurement system is illustrated in Fig. 4. The HEB device is stuck to the flat surface of a Si elliptical lens which has a long axis length of 5.228 mm and a minor axis length of 5 mm, the extension length is 1.149 mm. The lens, without anti-reflection coating, is mounted in a cupreous mixer block which is mounted in a close-cycled cryostat. A Zitex G104 film is used to filter the infrared radiation and a HDPE sheet with a thickness of 1.5 mm is employed as the vacuum window of the cryostat. The LO and RF signals are coupled to the HEB mixer by a 25 μm Mylar film. The LO signals are provided by a signal generator together with different frequency multiplier chains.

The intermediate frequency (IF) output signal from the HEB mixer is amplified firstly by a low noise amplifier (LNA) and then a room temperature amplifier. The amplified IF power is then filtered by a bandpass filter (80 MHz) at 1.5 GHz and recorded by a square-law detector.

Figure 3 shows the measured *I*–*V* curves of the HEB mixer at 0.2 THz and 0.85 THz with different local oscillator pumping levels. It is obvious that the well-pumped *I*–*V* curves at 0.2 THz still show negative resistances, which can be attributed to the non-uniformly absorption of LO power in the NbN micro-bridge.[14] The DSB noise temperatures T_{rec} have been measured at these pumping levels (shown in Fig. 3), and are then plotted in a two-dimensional graph of the bias voltage and current in order to get a better view of its dependence on bias points. At each fixed bias voltage, the noise temperature distribution corresponding to different bias currents (or LO pumping levels) is obtained by linear interpolation of the measured data.

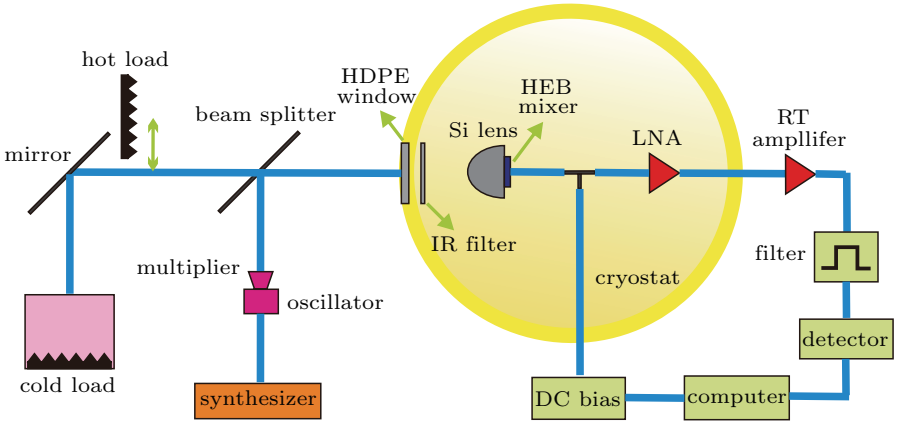


Fig. 4. Diagram of the noise temperature measurement setup.

3. Noise temperature distribution of superconducting HEB mixer

3.1. Optimal bias region

The DSB receiver noise temperatures have been measured at a large number of bias points at four frequencies, and are illustrated in Fig. 5. The effective radiation temperatures of 300 K and 77 K (blackbody) are calculated based on the Callen–Welton definition[15] at each LO frequency in the *Y*-factor method. What is more, the compensation of the direct detection effect is fulfilled by keeping the bias current unchanged between the 300 K and 77 K blackbody measurements.[16] A broad optimal bias range can be observed at each frequency, indicating a good bias applicability of the HEB mixer for multipixel application. Note that, the bias current of the HEB mixer (*Y* axis in Fig. 5) has been normalized to the critical current I_c for universal comparison. A raised region (marked by circle) at low bias voltage can be observed at 0.2 THz and 0.5 THz, which can be attributed to the negative resistance region as shown in the measured *I*–*V* curves. The lowest uncorrected DSB noise temperatures at these frequencies are also listed in Table 1, indicating that this HEB mixer has high sensitivity in the whole operating frequency range. The noise temperature at 1.34 THz is slightly higher than that at other frequencies, which is because the RF loss of 25 μm Mylar at 1.34 THz is higher than that at other frequencies (as shown in Table 2).

Table 1. Lowest uncorrected and corrected DSB receiver noise temperatures.

Frequency/THz	0.2	0.5	0.85	1.34
Uncorrected T_{rec}/K	720	720	750	900
Corrected T_{rec}/K	260	270	270	270

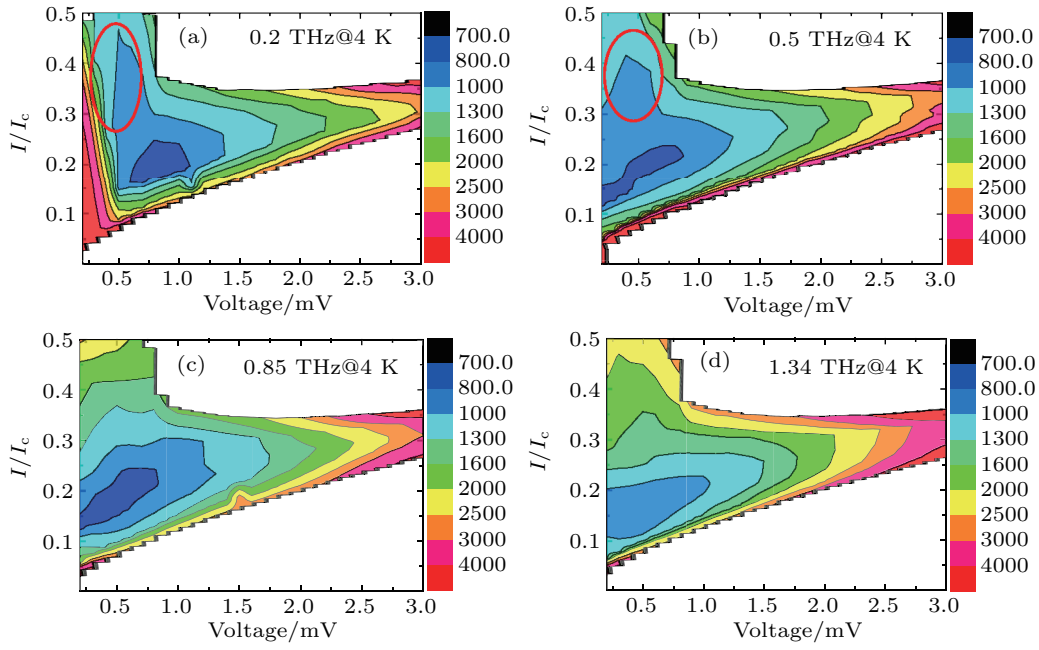


Fig. 5. Measured DSB receiver noise temperature T_{rec} in a two-dimensional graph of the bias voltage and current at (a) 0.2 THz, (b) 0.5 THz, (c) 0.85 THz, and (d) 1.34 THz. The isoline indicates the absolute value of T_{rec}.

Table 2. Loss of RF components.

Component frequency/THz	Beam-splitter/dB	Window/dB	IR filter/dB	Air path/dB	Si lens/dB	Antenna/dB
0.2	0.04	0.32	0.09	0.01	1.54	2.08
0.5	0.61	0.36	0.22	0.01	1.54	0.95
0.85	1.37	0.41	0.18	0.03	1.54	0.22
1.34	2.29	0.46	0.09	0.13	1.54	1.08

3.2. Frequency dependence of HEB mixer noise temperature

The measured DSB receiver noise temperature $T_{\rm rec}$ includes three parts: RF noise $T_{\rm RF}$, HEB mixer intrinsic noise $T_{\rm mixer}$, and IF noise $T_{\rm IF}$, and can be expressed as

$$T_{\rm rec} = T_{\rm RF} + \frac{1}{G_{\rm RF}}\left(T_{\rm mixer} + \frac{T_{\rm IF}}{G_{\rm mixer}}\right), \tag{1}$$

where $G_{\rm RF}$ is the RF loss, and $G_{\rm mixer}$ is the conversion gain of the HEB mixer. In order to investigate the distribution of HEB mixer noise temperature $T_{\rm mixer}$, we need to calibrate other noises.

The IF noise $T_{\rm IF}$ is mainly produced by the LNA and is normally very small (about 3–4 K). The conversion gain $G_{\rm mixer}$ of the HEB mixer is about -5 dB and is proved to be frequency independent.[14] Therefore we ignore the term $T_{\rm IF}/G_{\rm mixer}$ in Eq. (1) and focus on the calibration of RF loss $G_{\rm RF}$ and RF noise $T_{\rm RF}$.

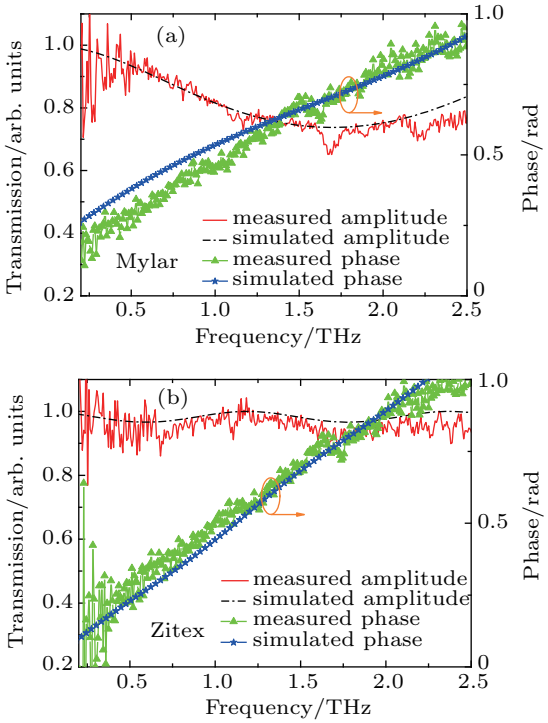


Fig. 6. Measured and simulated transmission of (a) 25 μm Mylar and (b) Zitex. Both amplitude (red solid line) and phase (green square line) are measured by a TDS, the simulated amplitude (black dash line) and phase (blue star line) are obtained by FEKO software with the measured permittivity.

The RF noise is produced by the RF optics in the receiver system which consists of a 25 μm Mylar beam splitter, a 1.5 mm HDPE window, a Zitex G104 infrared filter, an air path, a Si lens, and a planar spiral antenna. The equivalent input noise temperature $T_{\rm eq}$ of each RF component with a gain G is given by

$$T_{\rm eq} = T_{\rm cw}(T)(1-G)/G. \tag{2}$$

According to Eq. (2), the gain G of each RF component is the most crucial parameter. In order to obtain a precise value of the RF loss, we measure and simulate the transmittance of all RF components, as shown in Figs. 6 and 7. The transmittances of the Mylar and Zitex films are measured by a time-domain spectrometer (TDS), and the complex permittivity is derived from the measured result. The simulation of transmittance is performed by FEKO software[17] with measured complex permittivity, and as shown in Fig. 6 good agreement has been found between simulation and measurement. The transmittance of HDPE has been measured in Ref. [11]. The transmittance of the air path is calculated by an atmospheric model (AM).[18] The coupling efficiency between the planar spiral antenna and superconducting NbN film has been measured by a FTS with a calibration method described in Ref. [19]. The measured coupling efficiency of the spiral antenna shows

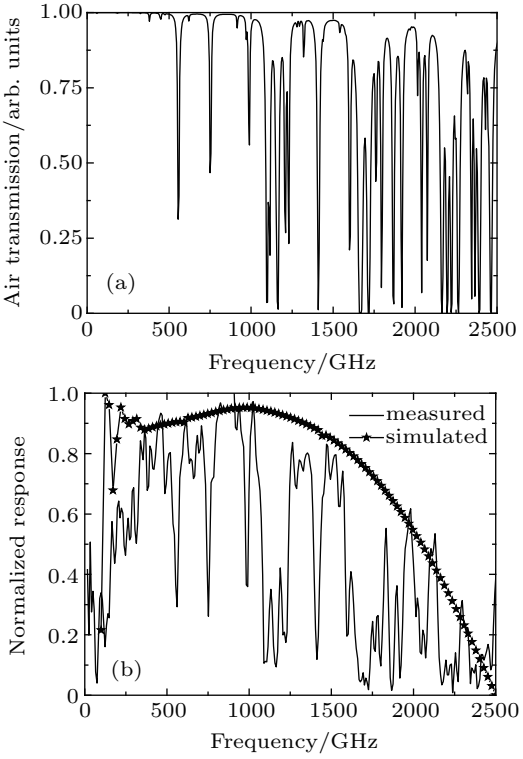


Fig. 7. (a) Simulated transmission of the air path in our lab by AM model. (b) Normalized coupling efficiency of spiral antenna by simulation and FTS measurement.

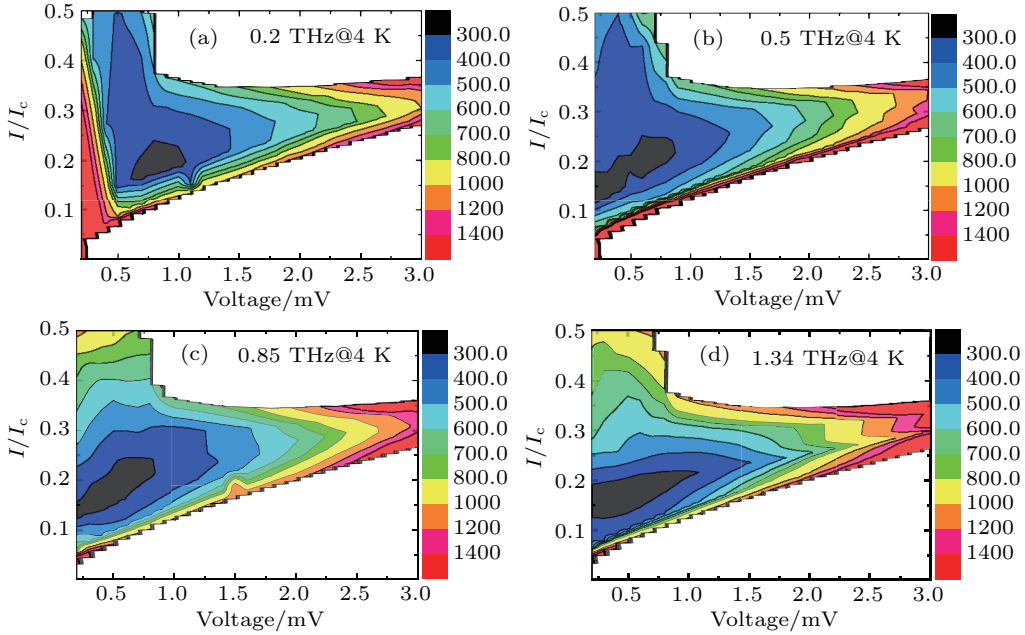


Fig. 8. Corrected HEB mixer noise temperature T_{mixer} in a two-dimensional graph of the bias voltage and current at (a) 0.2 THz, (b) 0.5 THz, (c) 0.85 THz, and (d) 1.34 THz. The isoline indicates the absolute value of T_{mixer}.

the same trend with the simulation one, where the difference is largely due to the water absorption in the air path, as shown in Fig. 7. The reflection loss of the air and Si lens interface on both sides is about 1.54 dB according to the measurements in Ref. [20], where the absorption loss inside the high resistivity silicon material is ignored. All measured and simulated RF losses are listed in Table 2.

After calibrating the RF noise and RF loss by Eqs. (1) and (2), we plot the HEB mixer noise temperature in a two-dimensional graph of the bias voltage and current at 0.2 THz, 0.5 THz, 0.85 THz, and 1.34 THz in Fig. 8. The corrected mixer noise temperature shows the same distribution on bias point at all frequencies, in other words a frequency independent optimal bias region has been observed. The corrected lowest noise temperature has also been listed in Table 1, a frequency independent mixer noise temperature has been obtained without considering the quantum noise contribution.

3.3. Bath temperature dependence

The receiver noise temperature of the superconducting HEB mixer has also been measured at 4 K, 5 K, 6 K, and 7 K to investigate the effect of the bath temperature on the optimal bias region. Figure 9 shows the DSB receiver noise temperatures distribution at different bath temperatures at 0.85 THz.

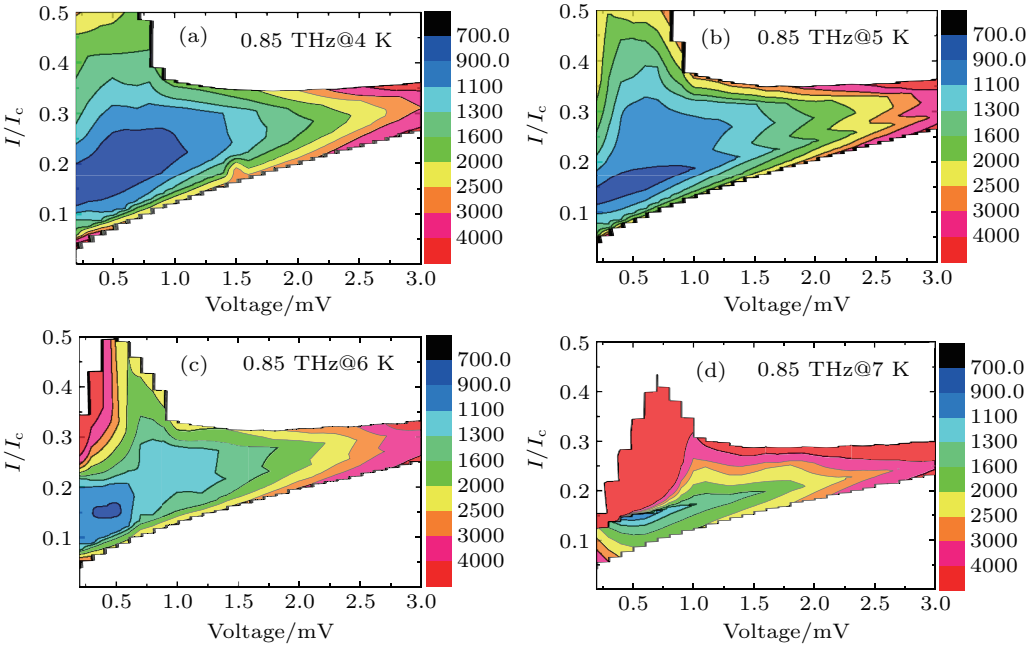


Fig. 9. Measured DSB noise temperature T_{rec} in a two-dimensional graph of the bias voltage and current at 0.85 THz at different bath temperatures.

Note that similar phenomenon has been observed at other frequencies, we only plot the result at this frequency for illustration. Figure 10 illustrates the bath temperature dependence of the measured results. The lowest receiver noise temperature $T_{\rm rec}$ only increases from 750 K to 810 K when the bath temperature increases to 6 K, however it rapidly raises to 1000 K when the bath temperature increases to 7 K due to the rapid decrease of the critical current of the HEB mixer. The optimal bias area, defined as the bias region where the noise temperature is lower than 900 K, has been calculated by counting the bias points with a voltage interval of 0.1 mV and a current interval of $0.01\times I/I_{\rm c}$. Obviously, the optimal bias points decrease rapidly with increasing bath temperature. In conclusion, we believe that the bath temperature has limited effect on the lowest receiver noise temperature until it raises to 7 K (about 0.8 times critical temperature $T_{\rm c}$[21]), however the optimal bias region deteriorates obviously with increasing bath temperature.

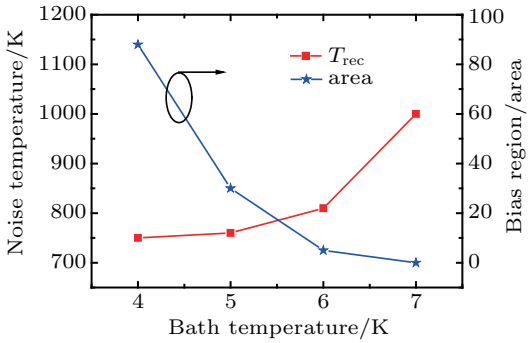


Fig. 10. Lowest receiver noise temperature (square) and optimal bias region (star) at different bath temperatures.

4. Conclusion

The noise temperature distribution of a wide-band superconducting HEB mixer has been investigated for the multi-pixel application. A broad optimal bias region has been observed at 0.2 THz, 0.5 THz, 0.85 THz, and 1.34 THz. The HEB mixer noise temperature has been calculated at all frequencies by calibrating the noise contribution of the RF components. The corrected mixer noise temperature has the same distribution on bias point at all frequencies, a frequency independent optimal region can be observed. The bath temperature dependence has also been investigated, the bath temperature has limited effect on the lowest receiver noise temperature $T_{\rm rec}$ until it raises to 7 K, however the optimal bias region deteriorates obviously with increasing bath temperature.

Acknowledgment

The authors are grateful to K. Zhang, Q. J. Yao, and W. Y. Duan of PMO for their assistance in the experiments.

References

[1] Gershenzon E M, Gol'tsman G N, Gogidze I G, Elant'ev A I, Karasik B S and Semenov A D 1990 *Sov. Phys. Supercond.* **3** 1582
[2] Meledin D, Pavolotsky A, Desmaris V, Lapkin I, Risacher C, Perez V, Henke D, Nystrom O, Sundin E, Dochev D, Pantaleev M, Fredrixon M, Strandberg M, Voronov B, Gol'tsman G N and Belitsky V 2009 *IEEE Trans. Microw. Theory Tech.* **57** 89
[3] Cherednichenko S, Drakinskiy V, Berg T, Khosropanah P and Kollberg E 2008 *Rev. Sci. Instrum.* **79** 034501
[4] Gu M, Kang L, Zhang L B, Zhao Q Y, Jia T, Wan C, Xu R Y, Yang X Z and Wu P H 2015 *Chin. Phys. Lett.* **32** 038501
[5] Li J, Wang M J, Shi S C and Matsuo H 2007 *Chin. Phys. Lett.* **24** 570
[6] Zhang Q Y, Dong W H, He G F, Li T F, Liu J S and Chen W 2014 *Acta Phys. Sin.* **63** 200303 (in Chinese)
[7] Huang Y R, Chiu C P, Lu W C, Chang H H, Chiang Y Y and Wang M J 2016 *Proceeding of URSI Asia-Pacific Radio Science Conference (URSI AP-RASC),* August 21–25, 2016, Seoul, South Korea, pp. 569–571
[8] Pütz P, Büchel D, Jacobs K, Schultz M and Honingh C E 2015 *Proceeding of 26th Int. Symp. Space THz Technology,* March 16–18, 2015, Cambridge, MA, USA
[9] Silva J R G D 2016 *Study on the viability of a* 4×2 *HEB mixer array at super-THz based on a Fourier phase grating LO for space applications* (Master Dissertation)
[10] Rigopoulou D, Caldwell M, Ellison B, Pearson C, Caux E, Cooray A, Gallego J D, Gerin M, Goicoechea J R, Goldsmith P, Kramer C, Lis D C, Molinari S, Ossenkopf-Okada V, Savini G, Tan B K, Tielens X, Viti S, Wiedner M and Yassin G 2016 *Proceeding of SPIE 9904, Space Telescopes and Instrumentation 2016: Optical, Infrared, and Millimeter Wave*, July 29, 2016, Edinburgh, United Kingdom, p. 99042K
[11] Shi S C, Paine S, Yao Q J, Lin Z H, Li X X, Duan W Y, Matsuo H, Zhang Q Z, Yang J, Ashley M C B, Shang Z H and Hu Z W 2016 *Nature Astronomy* 10001
[12] Zhu H T, Valentin J, Vacelet T, Herth E, Delorme Y and Wiedner M 2019 *Proceeding of 44th International Conference on Infrared, Millimeter, and Terahertz Waves (IRMMW-THz)*, September 1–6, 2019, Paris, France, pp. 1–2
[13] Ding J Q, Hu J, Shi S C and Zhao Y 2018 *IEEE Access* Vol. **6** pp. 42507–42515
[14] Miao W, Zhang W, Zhong J Q, Shi S C, Delorme Y, Lefevre R, Feret A and Vacelet T 2014 *Appl. Phys. Lett.* **104** 052605
[15] Kerr A R 1999 *IEEE Trans. Microw. Theory Tech.* **47** 325
[16] Baselmans J J A, Baryshev A and Reker S F 2005 *Appl. Phys. Lett.* **86** 163503
[17] *FEKO: A computer code for the analysis of electromagnetic problems*, EM Software & Systems-S.A. (Pty) Ltd., Stellenbosch, South Africa
[18] Paine S, *Am Atmospheric Model*, Available: https://www.cfa.harvard.edu/∼ spaine/am/
[19] Zhou K M, Miao W, Lou Z, Hu J, Li S L, Zhang W, Shi S C, Lefevre R, Delorme Y and Vacelet T 2015 *IEEE Trans. Appl. Supercond.* 25.3: 1–5
[20] Zhou K M, Miao W, Lefevre R, Delorme Y and Shi S C 2016 *Proceeding of URSI Asia-Pacific Radio Science Conference (URSI AP-RASC),* August 21–25, 2016, Seoul, South Korea, pp. 2010–2012
[21] Zhang W, Li N, Jiang L, Ren Y, Yao Q J, Lin Z H, Shi S C, Voronov B M, and Gol'tsman G N. 2007 *Proceeding of SPIE 6840, Terahertz Photonics 684007,* February 8, 2008, Beijing, China, p. 684007